Self-Generation of Chaotic Solitary Spin Wave Pulses in Magnetic Film Active Feedback Rings

Mingzhong Wu,[1] Boris A. Kalinikos,[2] and Carl E. Patton[1]
[1]*Department of Physics, Colorado State University, Fort Collins, Colorado 80523, USA*
[2]*St. Petersburg Electrotechnical University, 197376, St. Petersburg, Russia*
(Received 3 June 2005; published 28 November 2005)

The chaotic self-generation of short solitary spin wave pulses has been observed for the first time. The pulses were produced from parametrically excited spin waves in an yttrium-iron-garnet film in an active feedback ring under conditions where both three-wave and four-wave parametric processes were allowed. The power-frequency spectrum was broadband and chaotic.

DOI: 10.1103/PhysRevLett.95.237202 PACS numbers: 75.30.Ds, 05.45.−a, 76.50.+g, 85.70.Ge

There are two main focus areas in the study of nonlinear spin wave dynamics in magnetic system: (1) modulational instability and stationary nonlinear spin wave excitations in the form of envelope solitons; (2) chaotic nonlinear spin wave dynamics. The processes responsible for both classes of phenomena involve parametric magnon interactions through three- or four-wave processes.

For (1), much of the recent work has been on solitons in magnetic film active feedback ring (MFAFR) systems [1]. In particular, it has been demonstrated that yttrium-iron-garnet (YIG) film based rings are efficient systems for the stationary self-generation of both bright and dark envelope solitons. Most of this work was done at relatively high frequencies, typically above 4.5 GHz for in-plane magnetized YIG films, in order to eliminate three-wave processes and facilitate the formation of solitons through four-wave processes.

For (2), the main work has been on auto-oscillations, multistability, and routes to chaos through three-wave processes [2]. The end product chaotic signals had small bandwidths, typically in the 1 kHz–10 MHz range, much smaller than the width of the spin wave band. There has also been some work on chaos in YIG film feedback rings [3]. This work was done below 3 GHz where both three- and four-wave processes are allowed. The resulting chaotic signals had the same narrow-band character observed in the nonfeedback work.

This Letter reports first time results on the self-generation of broadband microwave regime chaotic spin wave signals in an MFAFR system. In contrast with the previous four-wave-only work on solitons [1] and three-wave-only work on chaos [2], this work was done in the coincidence regime [4] where both three- and four-wave parametric processes are allowed. In contrast with the previous MFAFR work on chaos [3], where only narrow-band spin wave excitations (< 10 MHz) were obtained, this work realizes continuous chaotic spin wave excitation essentially over the full nominally 1 GHz wide magnetostatic wave band. In the time domain, one obtains chaotic short pulses that appear solitary or isolated and have widths as narrow as a few nanoseconds. These results constitute the first continuous generation of chaotic short spin wave pulses by any means. This work shows that spin wave chaos from feedback ring structures provides new fundamental insight into chaotic nonlinear dynamics. This work can also have important applications to chaos based communications [5,6].

The experiments take advantage of the fact that a YIG film based feedback ring has many resonant modes. In the previous four-wave-only high field MFAFR work, only a few of the resonance modes were efficiently excited. This led to self-generated bright and dark soliton trains with limited bandwidths, typically below 150 MHz or so, much less than the full spin wave spectrum bandwidth. The new experiments show that one can increase the bandwidth of the self-generated waves by dropping the field into the coincidence regime where both three- and four-wave processes are allowed. If the initial ring modes are at levels above the three-wave parametric excitation threshold, these modes can parametrically excite new waves. Previous work has shown that for mode powers well above threshold, such excitations can provide various routes to chaos, among other things [2]. By extension, the ring resonance modes in an MFAFR structure operated in the coincidence regime should be able to generate parametric spin waves over a frequency range limited only by the bandwidth of the spin wave band. The data below show that this is really so.

Figure 1 shows the basic YIG film based MFAFR configuration. The ring consists of the YIG film strip with input and output microstrip transducers, a wide band linear microwave amplifier, and an adjustable attenuator for gain

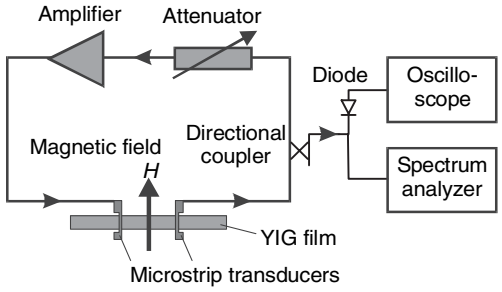

FIG. 1. Diagram of YIG film active feedback ring system.

 © 2005 The American Physical Society

control. The static magnetic field H is in the film plane and perpendicular to the strip length. The magnetostatic surface wave (MSSW) signals are excited and propagated in the YIG film. The output ring signal is sampled by a spectrum analyzer for frequency analysis and a diode detector and oscilloscope for temporal signal display.

The 9.2 μm thick, 1.3 mm wide, 35 mm long strip was cut from a larger single crystal YIG film grown by liquid phase epitaxy. This film had unpinned surface spins, a narrow ferromagnetic resonance linewidth of 0.4 Oe at 5 GHz, and a nominal saturation induction $4\pi M_s$ of 1750 G. The microstrip transducers were 50 μm wide and 2 mm long. For the selected data given below, the transducer separation L was held at 11 mm. Similar results were obtained for a range of L values from 2 to 15 mm.

Measurements were made in three stages. (1) The transmission loss versus frequency characteristics of the YIG film transducer structure and the frequency response of the entire ring at different gain values were measured for a range of H values over the four-wave only and the coincidence regimes. These data served to quantify the MSSW transmission response of the film, the ring resonance mode spectrum, and the defining frequency point below which one has coincidence. (2) Output power versus input power profiles were obtained for the YIG film alone for various field and input frequency combinations. These data provided the MSSW parametric instability threshold power levels in the coincidence regime. (3) Frequency spectra and time-domain waveforms for the ring signals were obtained for different fields and ring gain levels.

Figure 2 demonstrates the role of the field in shifting the spin wave bands to allow or disallow three-wave processes. The left side panels show measured transmission loss versus frequency response profiles for the YIG film structure with no feedback. These are juxtaposed against calculated spin wave dispersion curves in the right side panels. These panel sets are shown for two values of the static field H, as indicated. The transmission loss data are for a nominal input power of 8 dBm, well above the thresholds for three-wave processes. The dispersion curves are based on the standard spin wave theory for thin films with unpinned surface spins [7]. The S and B curves in the right side panels label the low k limit MSSW and magnetostatic backward volume wave (MSBVW) dispersion curves, respectively. The MSBVW modes have an in-plane wave vector that is parallel to the in-plane field. The wave number range for $k < k_{\max} \approx 10^3$ rad/cm is delineated by the vertical dotted line in the right side panels. Note that $k_{\max}$ defines the limit for the MSSW modes that can be efficiently excited with the microstrip transducer. The value of $k_{\max}$ is given by $4.8/w$, where w is the transducer width [8]. The horizontal dotted lines and ω labels indicate the MSSW band of supported frequencies. The pair of horizontal dashed lines in each right side panel and the $\omega/2$ labels show the cut at one-half the frequency of the modes within the MSSW band.

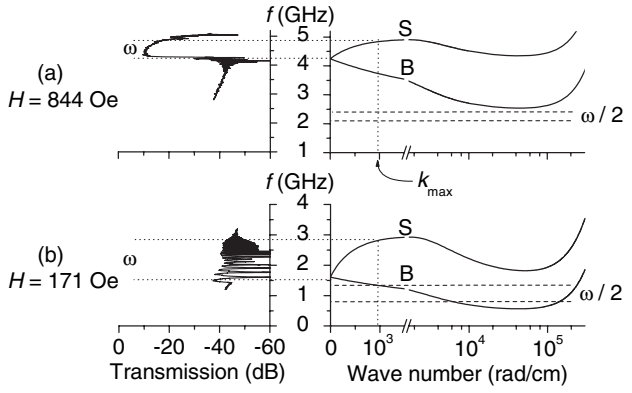

FIG. 2. Measured transmission versus frequency profiles (left panels) and computed spin wave dispersion curves of frequency versus wave number (right panels) for two values of the field H, as indicated. The vertical and horizontal lines and the S, B, $k_{\max}$, ω, and $\omega/2$ labels mark band limits and frequency bands relevant to three- and four-wave processes.

The two panels show the way in which a field change allows one to tune in or out the half frequency MSBVW modes, and hence, three-wave processes. (a) For $H =$ 844 Oe, there are no $\omega/2$ modes connected to the MSSW band. Here, one does see the expected region of large signal transmission, in the -10 to -20 dB range, across the MSSW band. (b) For $H = 171$ Oe, the full half frequency band corresponds to allowed MSBVW modes and all of the MSSW modes are parametrically unstable. Hence, the transmission is highly attenuated over the MSSW band. The parametric instability effect due to the availability of half frequency modes and three-wave processes is clearly present. Measurements as a function of input power gave typical three-wave process thresholds in the $-10 \sim -20$ dBm range.

It is the low field, Fig. 2(b), coincidence regime that is of interest here. With feedback and sufficient gain for the setup in Fig. 1, one can maintain a reasonable ring power even in the three-wave regime shown in the Fig. 2(b) panel. Then, as the gain is increased, one observes the gradual development of a broadband chaotic response. Figures 3–5 show representative results. All three figures show power-

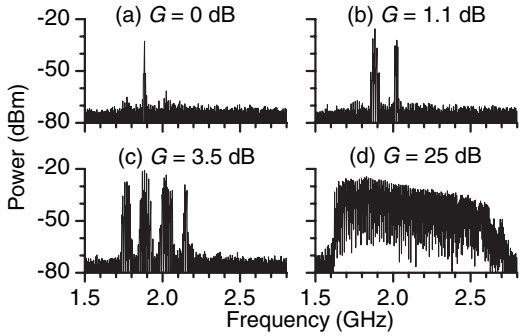

FIG. 3. Power-frequency spectra for different ring gain G values, as indicated. The static field was 171 Oe, the same as in Fig. 2(b).

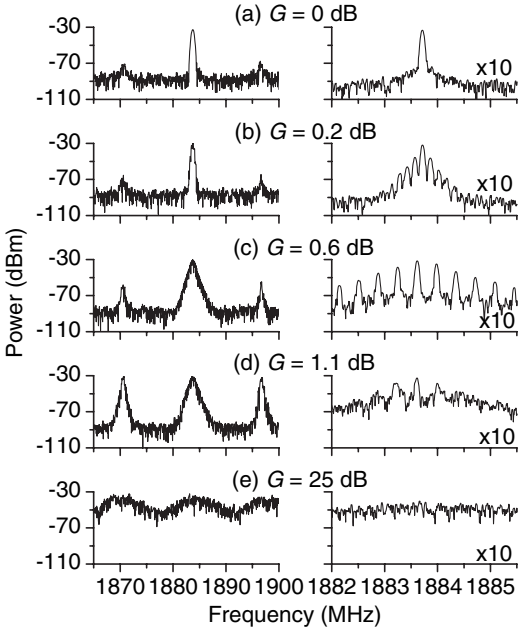

FIG. 4. Power-frequency spectrum development for frequencies close to that of the dominant ring mode at gain $G = 0$ dB as a function of the ring gain, as indicated. Graphs are shown for two frequency scales, 35 and 3.5 MHz, in order to show the simultaneous development of the four-wave ring mode frequencies (left graphs) and the fine structure and drive to chaos associated with the additional three-wave processes (right graphs).

frequency (PF) spectra for the setup of Fig. 1 with the field set at 171 Oe, the same as for Fig. 2(b), as the feedback gain G is gradually increased from the $G = 0$ dB point at which the system just supports one resonant ring mode. This mode gives the lowest threshold for oscillation in the ring. Figure 5 also shows the temporal chaotic pulse response that one obtains at the highest available gain, where the PF spectrum is chaotic over the full MSSW band.

Figure 3 shows the evolution of the MSSW passband PF spectrum with increasing gain. At the $G = 0$ dB threshold,

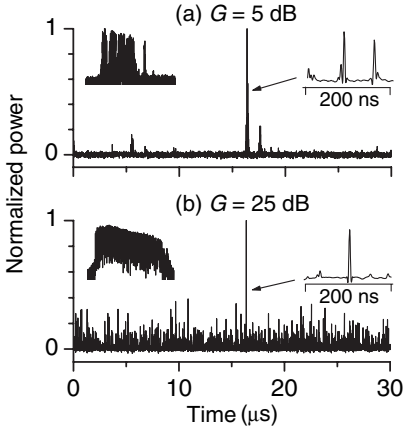

FIG. 5. Time trace envelope waveforms on a 30 μs time scale for two different ring gain G values, as indicated. The left insets show corresponding power-frequency spectra. The right insets show expanded time traces.

the ring produces a cw signal for the lowest loss ring mode. With increasing gain, more and more harmonics are generated and the spectrum is broadened and enriched. Finally, at $G = 25$ dB, the spectrum widens to about 1000 MHz and is more or less continuous. This width matches the full width of the MSSW band at $H = 171$ Oe. The coincidence regime response in Fig. 3 is in significant contrast to the response when only four-wave processes are allowed. In the four-wave-only case, the ring response at high gain shows only a regular comb frequency profile with a width that is typically less than 150 MHz [1]. In the coincidence regime, this sharp comb structure does make an appearance at intermediate gains, but the profiles are modified significantly by the addition of the three-wave processes.

Figure 4 shows data on the spectrum development with increasing gain G, as indicated, for frequencies close to that of the single dominant ring mode at $G = 0$ dB in Fig. 3(a). The left side graphs are for a frequency span of 35 MHz; while the right side graphs are for a $\times 10$ expanded scale. The expanded scale shows the fine structure associated with the resolution limited spectra in the left side graphs.

For the $G = 0$ dB (a) graphs, the spectrum shows one center peak only, as in Fig. 3(a). As the gain is increased, there are two changes. First, as shown in the left graph sequence, side lobes develop at about 13 MHz to either side of the main peak. All of these peaks then broaden and merge as the gain is increased. Second, as shown in the right side graphs, the central peak itself develops a fine comb structure with about a 0.2 MHz spacing. This structure also broadens and eventually washes out into a chaotic response at the highest gain. The lower left graph shows that this chaotic response still retains a semblance of the side lobe structure found for lower gains.

These data show the detailed interplay of four-wave and three-wave processes. The initial side lobes that develop in the left side graph sequence are due to the ring resonances in combination with four-wave modulational instability processes. The frequency spacing derives from the round-trip circulation time period for the ring modes, $\tau = L/\nu_g + \tau_e$, where L/ν_g is the propagation time for a spin wave packet with group velocity ν_g and τ_e is the signal propagation time in the rest of the ring. For the present setup, ν_g is about 16×10^6 cm/s at 1884 MHz and τ_e is about 8 ns. These values give at of 77 ns and a $1/\tau$ of 13 MHz. The broadening that occurs with increasing gain is due to three-wave processes. It is important to emphasize, yet again, that at higher magnetic fields where three-wave processes are excluded, one sees only the development of this frequency comb, with frequency peaks that remain sharp and develop no fine structure as the power is increased [1].

In the low field case considered here, coupling between the self-generated spin waves through four-wave processes, in combination with the coupling between these modes and the half frequency spin waves through the three-wave processes, provides the key to the new effect of

broadband chaos shown in the right side bottom graphs in Fig. 4. As noted, the frequency spectrum of the self-generated signal loses its regular four-wave comb character as the fine structure and chaotic broadening develop. The frequency spectrum evolution for the ring signal shown here is typical of that for the other main peaks that appear at higher gains as well.

The large scale and fine scale frequency comb development shown in Figs. 4(b) and 4(c), demonstrate an entirely new dual modulation effect. The combined four- and three-wave processes then give the broad and chaotic spectrum shown in Figs. 3(d) and 4(e). While the spectrum for the self-generated signals appear to be more or less continuous at the highest gains, this is not really so. This is because the selection rules for the modes involved in the three-wave processes support only discrete half frequency mode pairs [9]. It is important to stress that, even though the initial cw mode is initiated from ring thermal noise, the clean spectra in Figs. 4(a)–4(c), conclusively demonstrate the coherent behavior of the self-generated spin wave signals. The observed chaos evolved from those coherent waves rather than from noise.

Perhaps the most intriguing aspect of the current results concerns the nature of the wide band chaotic signals in the time domain. The high power limit spectra in Figs. 3 and 4 lead to signals in the form of a chaotic sequence of narrow pulses. The amplitudes of these pulses and the time separations between neighboring pulses show chaotic behavior. The individual pulses are extremely narrow, in the nanosecond range. The time separations for the largest amplitude pulses are typically in the range of 50 μs or more.

Figure 5 shows examples of these signals. The (a) and (b) graphs show pulse envelope power versus time traces for two gain values, $G = 5$ dB and $G = 25$ dB, as indicated. Note the long time scale of 30 μs for the time trace axes. The left insets show the companion PF spectra on frequency scales that match those in Fig. 3. The right insets show expanded time traces for the largest spikes in the main graphs. For (b), the PF spectrum is the same as in Fig. 3(d). The time traces were obtained in a single shot mode. Because of the chaotic nature of the generated signal, the details of every time trace are different.

Both graphs show chaotic temporal pulses. For (a), because of the more discrete PF spectra, the individual pulses actually have structure. The inset shows that the peak is actually composed of multiple peaks. The spacing of these peaks actually matches the original ring resonance propagation time τ. This shows that in the quasichaotic intermediate gain regime, the ring resonance response still maintains a presence. The width of the individual pulses in the inset is in the range of 3–4 ns.

For the $G = 25$ dB gain situation in (b), the evolution from a quasidiscrete PF spectrum to a broadband chaotic spectrum over the full MSSW band produces a significant change in the temporal response. One now obtains a self-generated time domain signal that may be described as a sequence of ''solitary'' pulses. As shown in the lower inset, this solitary peak is now indeed solitary. There is no longer any remanence of the peak structure shown in the inset of (a). These solitary pulses are generated chaotically. As in (a), the pulses are very narrow, on the order of a few ns. These data give the last key result of this work, a chaotic narrow pulse sequence with more or less continuous, but yet discrete chaotic PF spectrum. The broad width of the PF spectrum that extends over the entire MSSW band defines the narrow width of the time-domain pulses. At the same time, the chaotic nature of the spectrum leads to the intriguing time domain response in the form of chaotic solitary pulses.

In summary, this Letter reports the first experimental observation of the self-generation of (a) broadband chaotic spin wave signals in the frequency domain and (b) narrow solitary chaotic pulses in the time domain. The experiments utilized a yttrium-iron-garnet film in a feedback ring in the range of excitation frequencies where both three- and four-wave parametric processes are allowed. A thorough understanding of these new phenomena demands new theoretical work, possibly through full nonlinear analyses based on the Landau-Lifshitz and Maxwell equations [10] or through a Hamiltonian formalism [11] adapted for thin magnetic films.

This work was supported in part by the U. S. Army Research Office, DAAD19-02-1-0197 and W911NF- 04-1-0247, the National Science Foundation, DMR-0108797, and the Russian Foundation for Basic Research, 05-02-17714.

[1] B. A. Kalinikos, N. G. Kovshikov, and C. E. Patton, Phys. Rev. Lett. **80**, 4301 (1998); B. A. Kalinikos, M. M. Scott, and C. E. Patton, Phys. Rev. Lett. **84**, 4697 (2000); A. A. Serga, S. O. Demokritov, B. Hillebrands, and A. N. Slavin, Phys. Rev. Lett. **92**, 117203 (2004).

[2] P. H. Bryant, C. D. Jeffries, and K. Nakamura, Phys. Rev. A **38**, 4223 (1988); T. L. Carroll, L. M. Pecora, and F. J. Rachford, Phys. Rev. A **40**, 377 (1989); F. M. de Aguiar A. Azevedo, and S. M. Rezende, J. Appl. Phys. **73**, 6825 (1993).

[3] V. E. Demidov and N. G. Kovshikov, Tech. Phys. Lett. **24**, 274 (1998); Tech. Phys. Lett. **24**, 647 (1998).

[4] H. Shul, J. Phys. Chem. Solids **1**, 209 (1957).

[5] A. S. Dmitriev *et al.*, Int. J. Bifurcation Chaos Appl. Sci. Eng. **13**, 1495 (2003).

[6] See, e.g., Special Issue of IEEE Trans. Circuits Syst. I **48**, 12 (2001).

[7] B. A. Kalinikos and A. N. Slavin, J. Phys. C **19**, 7013 (1986).

[8] V. F. Dmitriev and B. A. Kallnikos, Izv. Vyssh. Uchebn. Zaved., Fiz. **31**, 24 (1988) [Sov. Phys. J., **31**, 875 (1988)].

[9] V. T. Synogach *et al.*, Phys. Rev. Lett. **85**, 2184 (2000).

[10] A. G. Gurevich and G. A. Melkov, *Magnetization Oscillations and Waves* (CRC, New York, 1996).

[11] V. S. L'vov, *Wave Turbulence Under Parametric Excitation* (Springer-Verlag, Berlin, 1994).